# Semi-analytical Equations for Designing Terahertz Graphene Dipole Antennas on Glass Substrate

Marcos E. C. Garcia[1] , Rodrigo M. S. de Oliveira[1] , Nilton R. N. M. Rodrigues[1] ,
[1]*Federal Institute of Pará (IFPA), Belém, Pará, Brazil, marcos.garcia@ifpa.edu.br, rmso@ufpa.br,
niltonrodolfo@ufpa.br*

*Abstract*— **Semi-analytical equations are developed for aiding the process of designing terahertz graphene-based rectangular dipole antennas lying on glass substrates. It directly provides the dipole length required for obtaining resonance at a desired frequency since antenna width and graphene chemical potential are known. By using the finite-difference time-domain (FDTD) method, a large number of computational simulations were performed considering several combinations of antenna dimensions and chemical potential values. The simulation results were used along with graphene electrostatic scaling law combined with the least squares method to optimize the formulation coefficients. With the optimized coefficients, we obtain very satisfying accuracy levels. In the frequency range from 0.5 THz to 3.0 THz, the average relative absolute error is 1.50%, with maximum relative absolute error of 6.77%.**

*Index Terms*— Graphene Dipole Antenna, Engineering Design, Resonance Frequency, Terahertz Radiation.

## I. INTRODUCTION

Graphene is a single layer of carbon atoms forming a honeycomb-like lattice. For many years, one believed that strictly two-dimensional crystals could not exist and graphene was treated as a theoretical material [1]. Since the successful isolation of a graphene sheet in 2004 [2], it has attracted the growing interest of the industry and research communities in several fields [3] due to its remarkable physical properties [1] [4].

In the field of wireless communication systems, graphene has opened doors for designing small terahertz (THz) antennas [5]. The main reason is that the physics of this material enables Surface-Plasmon Polariton (SPP) waves in the THz range (0.1-10 THz) [6] [7]. Such property allows graphene antennas with dimensions of just a few micrometers to resonate in THz range, which are up to two orders of magnitude below the necessary length of a classical metallic antenna [8]. This frequency band is between the microwave and optical bands, which are spectrum regions with well-developed technologies. In comparison with microwave and optical bands, THz devices are still in their early developments [9] [10]. Therefore, it is an exceptional opportunity of achieving terabit-per-second transfer rates wirelessly [11]. Another interesting characteristic of a graphene sheet is its electrical conductivity, which can be controllably tuned by adjusting graphene chemical potential, which is in turn set by adjusting external electrostatic field [12]. This is made by applying a gate voltage $V_{DC}$ [13] between the graphene sheet and an electrode of a transparent material such as PEDOT:PSS [14] (see Fig. 1(c)). For a given $V_{DC}$, $|\mu_c| \approx v_f \hbar \sqrt{(\pi \varepsilon |V_{DC}|)/(q_e G_e)}$, in which $v_f$ is the Fermi velocity, $\hbar$ is

the reduced Planck constant, $q_e$ is the elementary charge and $G_e$ is the gate extent [13]. This feature provides the means to tune the resonance frequency of a graphene-based terahertz antenna [15]–[17].

Some early works ignored the necessity of a feeding mechanism and studied graphene nano-patches operating in receiving mode [18]–[20]. Further efforts on modeling transmitting graphene antennas led to the study of classical antenna engineering parameters. A pin feed was proposed in [21], along with the first simulation study of a transmitting freestanding graphene nano-patch antenna. The radiation patterns were demonstrated to be very similar to that of a half-wavelength electric dipole antenna. The dipole structure is one of the simplest forms of resonant graphene antenna, set up over a glass substrate ($\varepsilon_r = 3.8$), which was first proposed in [16]. The main difference between the antennas proposed in [16] and [21] is the addition of a lumped source between graphene sheets to excite the dipole antenna in [16], allowing one to study its input impedance, resonance frequency, radiation efficiency, and radiation patterns, since the device operates in transmitting mode. The results in [16] were obtained with a full-wave solver and later they were validated in [22] using a therein proposed finite-difference time-domain (FDTD) graphene modeling method based on piecewise linear recursive convolution [23] and on thin material sheets [24] techniques.

Reconfigurable antennas have additional levels of functionality with important applications, such as the ability to dynamically modify their operation band [25] and radiation properties [26]. In [27], it was numerically demonstrated that the resonance frequency $f_r$ of a graphene dipole antenna can be tuned by adjusting the graphene chemical potential. The reconfigurable antenna proposed in [27] uses stacked graphene patches and can tune the resonance frequency from 0.8 to 1.8 THz. Soon after, a miniaturized dipole graphene antenna was designed in [28] to have an operating band that is tunable between 0.8 and 1.6 THz. A circuit model for rectangular tunable graphene dipoles was proposed in [29]. Results in [29], improved with fitting procedures, accurately predict the input impedance for an antenna with the same fixed geometrical parameters used in [27], for different levels of chemical potential. A photoconductor placed between two coplanar graphene sheets, forming a dipole, feeds the antenna in [30]. This technique works by exciting the photoconductive material with an optical laser operating in pulsed mode. This source has high impedance, in the order of magnitude of typical THz graphene dipole input impedance, favoring impedance matching [30].

As graphene has an one-atom-thin nature, it must be supported on a substrate when it is used for designing real devices [31]. One of the most common substrates used in graphene-based experiments is the SiO$_2$ glass ($\varepsilon_r = 3.8$) [31] [32] because it has high chemical stability and very strong adhesion to graphene [31] [33]. The graphene/glass combination permits optically transparent antennas which can be installed on windows, eyeglasses, and cellphones displays preserving their transparency [34]. Furthermore, substrates with the same permittivity are used in several graphene-based antennas studies [17] [35]–[37]. Different substrates are studied in [38] and simulations show that the dipole graphene antenna with quartz ($\varepsilon_r = 3.75$) substrate stands out with the so far most interesting results for return loss, radiation efficiency, bandwidth, and directivity at a targeted resonance frequency of 1.02 THz. References [39] and [40] present a method that combines the method of moments with a generalized equivalent circuit to compute the input impedance and other parameters of a graphene dipole antenna. The method approximates a 3D problem to a 2D problem. For validation, the same structure proposed in [41] was modeled with the method presented in [39] and [40], leading to approximate results. A miniaturized reconfigurable dipole graphene antenna presented in [17] shows improved performance

parameters, such as return loss, multi-resonance, bandwidth, radiation efficiency, and tunable resonance frequency (from 0.912 to 6.279 THz), compared to previous devices in literature. A novel THz $4\pi$ band-edge oscillator based on a two-mode operation concept designed and fabricated in [42] seems to be an interesting approach for THz radiation sources, although it currently requires large and heavy hardware. Therefore, using a photomixer to feed a graphene antenna is an appropriate option today in terms of practical and compact wireless transmitting THz devices.

In literature, few studies provide formulas related to the prediction of the resonant frequency of Terahertz graphene dipole antennas. A simple formula based on a Fabry-Perot model is used in [19] for fast estimation of the resonance frequency of a graphene-based nano-patch antenna as a function of its length. The antenna is modeled as an infinitely wide graphene patch suspended in the air. The results are validated with numerical simulations performed using the method of moments and the surface equivalence principle. A realistic graphene-based nano-patch antenna, however, will have a finite width. A partial element equivalent circuit (PEEC) model [43], which is a relatively complicated method, was presented for graphene patches. The method can be used to calculate the frequencies at which there are absorption cross section peaks, that are regarded as the resonant frequencies. The approach in [43] was validated using results from [15] and [44] and since its formulation is based on single graphene patches, it does not take into account feeding mechanisms. In [35], it was proposed an equivalent RLC resonant circuit model for graphene-based bowtie antenna fed by a THz photomixer between the two arms. Recently, it was developed in [37] a circuit model for nanoscale graphene dipole antennas. However, circuit models lack the capability of providing operational characteristics of antennas, such as their resonance frequencies, from geometric and material parameters of the devices. Furthermore, the parameters of circuit models need to be extracted from simulation data.

In this work, a new semi-analytical formulation is proposed, which is capable of predicting graphene dipole length required for obtaining a desired resonance frequency, given the antenna width and chemical potential. It is based on graphene electrostatic scaling law [45] [46], which has been combined with the least squares method for performing the optimization of formulation coefficients. For this goal, it was made an extensive study of the resonance frequency behavior for several lengths and widths of the graphene rectangular dipole and several chemical potential levels applied to the graphene patches, using structures based on the graphene dipole antenna model proposed in [16]. To obtain the input impedance of the antenna in the frequency range of interest for each of the different combinations of parameters, the FDTD method [22] was used. FDTD method was chosen because it requires much less computational resources than frequency domain techniques when a wide-band analysis is required [47]. The formulation presented in this paper can be used to support and simplify the design of future graphene dipole antennas. The main advantages are: the formulation parameters are precalculated (no need for further numerical simulations), the model has finite widths and the influence of the source mechanism is taken into account. With the aim of maximizing radiation efficiency, we suggest the use of a photomixer with a graphene-based emitter proposed in [48] that is capable of matching the antenna's input resistance by adjusting its internal Fermi energy.

The remainder of this paper is organized as follows. In section II, the FDTD formulation used in this work is reviewed. Numerical results regarding the first resonance frequency of graphene dipole antennas are presented in Section III. In Section IV, details of the calculation of the plasmonic phase constant of the graphene are presented, which is necessary for predicting the total length of the graphene dipole
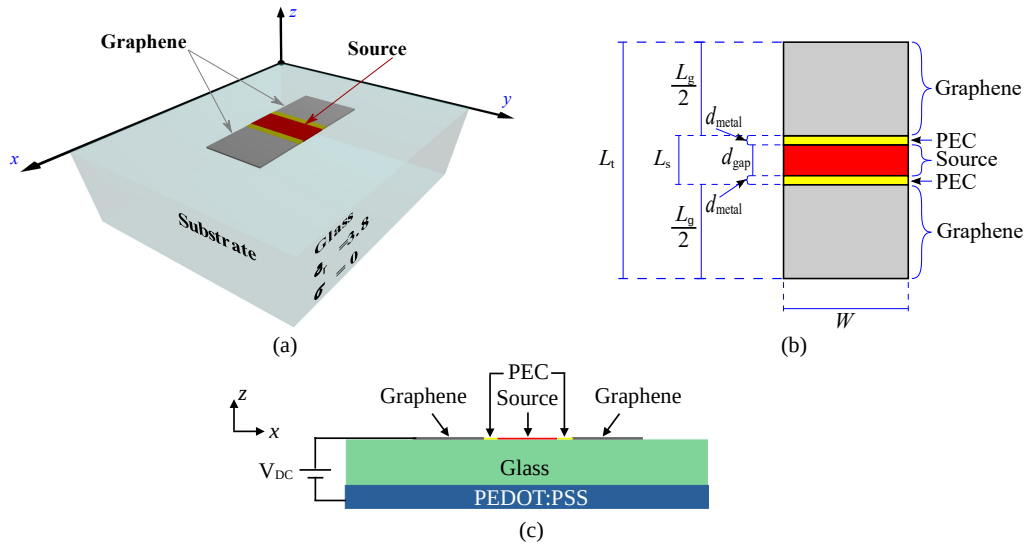
Fig. 1. Geometry of the studied graphene dipole antenna: (a) the schematic in a perspective view, (b) antenna dimensions and (c) mechanism for tuning graphene chemical potential.

antenna at a given first resonance frequency. In Section V, the accuracy of the proposed formulation is calculated and discussed. To obtain maximum radiation efficiency, an impedance matching approach is suggested in Section VI. Final remarks are drawn in Section VII.

## II. REVIEW OF THE FDTD FORMULATION USED FOR PERFORMING SIMULATIONS

To perform the numerical studies, the FDTD formulation developed in [22] was used in this work. FDTD is a relatively simple but powerful full-wave method, widely used for analyzing problems of electrodynamics [47].

Since the thickness of graphene is that of a carbon atom, for graphene structures with dimensions in micrometers one can consider a surface conductivity model for infinitely-large graphene sheets [12] [49]. Graphene patches can be modeled using Kubo's formula, which determines its complex conductivity $\widetilde{\sigma}(\omega)$ with appropriated precision level. Within the frequency band of interest ($0.5 - 4.0$ THz), Kubo's formula can be approximated neglecting the interband term and considering only the intraband contribution [12] [15], which is given by

$$\widetilde{\sigma}(\omega) = \frac{\sigma^*}{d}\left(\frac{1}{j\omega + 2\Gamma}\right). \tag{1}$$

In (1), $d$ is the graphene sheet's thickness, $\Gamma$ is the scattering rate $\Gamma = 1/(2\tau_0)$, where $\tau_0$ is the relaxation time, and $\sigma^* = \frac{q_e^2 k_B T}{\pi \hbar^2}\left(\frac{\mu_c}{k_B T} + 2\ln\left(1 + e^{-\mu_c/k_B T}\right)\right)$, where $q_e$ is the electron's charge, $k_B$ is the Boltzmann constant, $T$ is the temperature, $\hbar$ is the reduced Planck's constant, and $\mu_c$ is the chemical potential. In this work, $\tau_0 = 1$ ps and $T = 300$ K (the same parameters considered in [16]).

To execute electromagnetic simulations involving graphene using the FDTD method, it is necessary to embed a thin graphene sheet in the 3D lattice. The model demonstrated by [24] was used for that in [22], from which it is obtained an effective conductivity $\widetilde{\sigma}_{\text{eff}} = (d/\Delta_{x,y,z})\widetilde{\sigma}$, where $\Delta_{x,y,z}$ is the spatial step of the FDTD lattice set up with cubic cells. Analytic inverse Fourier transformation is used

to obtain the time domain equivalent of the effective conductivity, which is given by

$$\sigma(t) = \frac{\sigma^*}{\Delta_{x,y,z}} e^{-2\Gamma t}, \qquad t > 0. \tag{2}$$

The update equations of the fields are obtained from the differential form of Maxwell's equations

$$\frac{\partial \vec{D}}{\partial t} + \vec{J} = \nabla \times \vec{H} \tag{3}$$

and

$$\frac{\partial \vec{B}}{\partial t} = -\nabla \times \vec{E}, \tag{4}$$

where $\vec{D} = \varepsilon \vec{E}$ and $\vec{B} = \mu \vec{H}$. For calculating the current density on the graphene sheet, the convolution $\vec{J}(t) = \int_0^t \vec{E}(t-\tau)\sigma(\tau)d\tau$ can be used in the Ampère's law (3), that can be written as

$$\varepsilon \frac{\partial \vec{E}}{\partial t} + \left( \int_0^t \vec{E}(t-\tau)\sigma(\tau)d\tau \right) = \nabla \times \vec{H}. \tag{5}$$

The problem with (5) is that it is not suitable to be used directly with the FDTD method because the convolution, as given in (5), needs the electric field to be stored for all past time steps. This problem can be solved by using the technique Piecewise Linear Recursive Convolution (PLRC) [23], as described in [22]. Therefore, the FDTD equation used for updating tangential electric field components on graphene sheets is given by

$$E_\alpha^{n+1}(i,j,k) = \frac{\left( \nabla \times \vec{H} \right).\hat{\alpha} + \frac{\varepsilon(i,j,k)}{\Delta t} E_\alpha^n(i,j,k) - \frac{1}{2}\Psi_\alpha^n(i,j,k)}{\frac{\varepsilon(i,j,k)}{\Delta t} + \frac{1}{2}\sigma_0(i,j,k)}, \tag{6}$$

in which $\sigma_0 = (1 - e^{-2\Gamma\Delta t})\sigma^*/(2\Gamma\Delta_{x,y,z})$, $\alpha = x, y$ or $z$, and $\Psi_\alpha^n(i,j,k)$ is the previously mentioned convolution, which is recursively calculated by using the PLRC accumulator

$$\Psi_\alpha^n(i,j,k) = E_\alpha^n(i,j,k)S_0(i,j,k) + e^{-2\Gamma\Delta t}\Psi_\alpha^{n-1}(i,j,k), \tag{7}$$

where $\Psi_\alpha^0(i,j,k) = 0$ and $S_0 = (1 - e^{-4\Gamma\Delta t})\sigma^*/(2\Gamma\Delta_{x,y,z})$. One can notice from (7) that the PLRC accumulator needs to store the electric field of a single previous time iteration for time-advancing the convolution.

## III. FIRST RESONANCE FREQUENCY OF GRAPHENE DIPOLES

In this section, numerical results of the first resonance frequency of graphene dipole antennas are presented for various levels of graphene chemical potential $\mu_c$ and for several combinations of antenna's dimensions $L_t$ and $W$. Such as indicated in Fig. 1(b), $L_t$ is the total length of the graphene dipole antenna and $W$ is its width. The dimensions $L_t$ and $W$ of the antenna range from 9 to 91 μm and from 1 to 32 μm, respectively. Every simulation was performed using the FDTD method with cubic Yee cells, of which edges measure $\Delta_{x,y,z} = 0.5$ μm. The CPML technique [47] was used to truncate the computational domains of the 2178 electromagnetic simulations executed to obtain the data presented in this work.

For each simulation, the input impedance $Z$ of the graphene dipole antenna is obtained such as described in [22]. Figure 2 illustrates $Z$ for cases in which $L_t = 15$ μm and $W = 2$ μm, considering three different values of $\mu_c$: 0.2, 0.4 and 0.6 eV. The first resonance frequency for each case is indicated

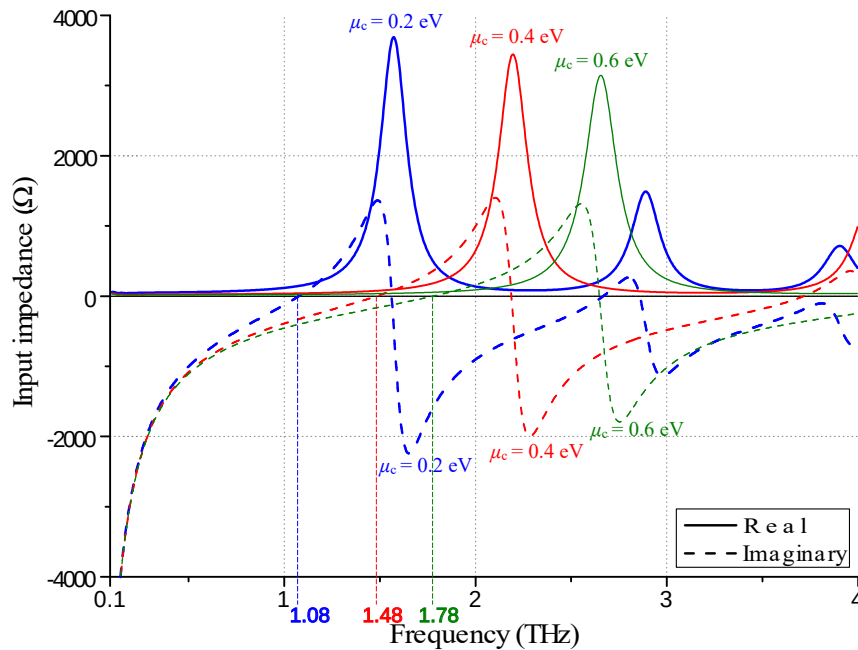Fig. 2. Input impedances of graphene dipole antenna measuring $W = 2$ μm and $L_t = 15$ μm, with $\mu_c$ set to 0.2, 0.4 and 0.6 eV.

in Fig. 2, which are, respectively, 1.08, 1.48, and 1.78 THz. It is seen that the dipole first resonance frequency, which is the smallest frequency at which the antenna reactance $\text{Im}\{Z\}$ is equal to zero, increases with $\mu_c$.

By numerically calculating the first resonance frequency of the several structures simulated in this work, it is possible to plot curves that show the influence of each antenna parameter. Figure 3 indicates that the antenna length $L_t$ must decrease nonlinearly as desired resonance frequency increases. Furthermore, for a fixed value of $L_t$, the increasing of $W$ slightly increases the first resonance frequency, while the increasing of $\mu_c$ significantly shifts the resonance frequency for higher values. To illustrate the advantage of using the equations proposed in this work, notice that the time to run an FDTD simulation for a dipole antenna with $W = 1$ $\mu m$ and $L_t = 12$ $\mu m$ is 15 minutes. For the case in which $W = 32$ $\mu m$ and $L_t = 90$ $\mu m$ the processing time is 90 minutes. All simulations were coded in programming language C and executed by using one core of a computer with an i5-9400F processor with clock up to 4.10 GHz. The 64-bit Linux operating system has been used.

From a theoretical point of view, the calculation of resonance frequency $f$ of graphene dipole antennas has similarities to that of metallic dipole antennas. As a rough first approximation, due to the not negligible source and metallic parts dimensions, the device consists of a pair of quarter-wavelength graphene sheets placed end to end with a total length of approximately $L_t = \pi/\beta$, where $\beta$ is the phase constant of the finite-width plasmonic strip [16].

The metallic electrodes separated by a gap form a coplanar plate capacitor with capacitance given by [50] [51]

$$C = \varepsilon_{\text{eff}} W \frac{K\left(\sqrt{1 - k^2}\right)}{K(k)}, \tag{8}$$

where $\varepsilon_{\text{eff}} = \varepsilon_o(1 + \varepsilon_r)/2$ is the surrounding effective permittivity, $W$ is the width of the antenna, $K(.)$
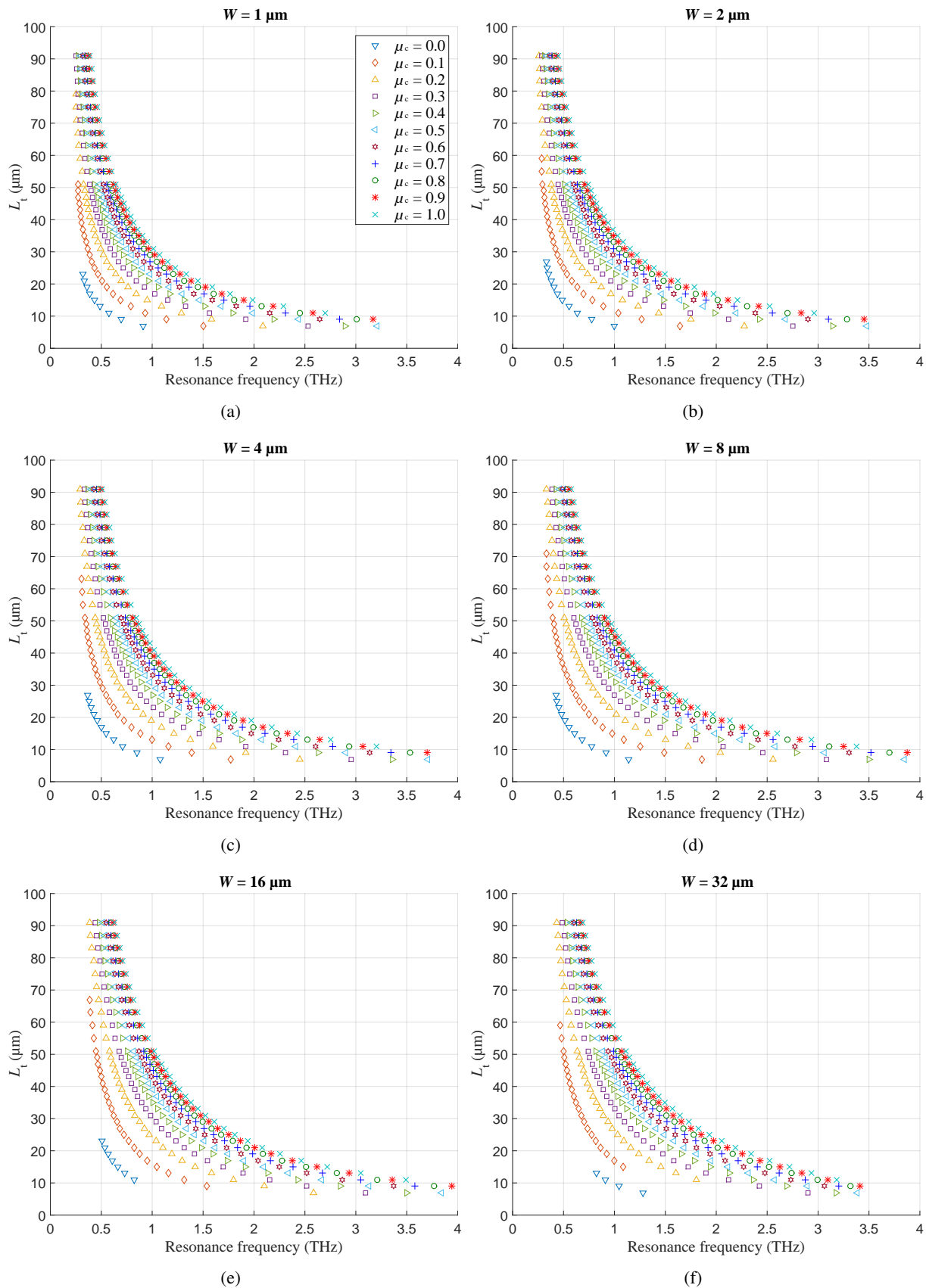
Fig. 3. Graphene dipole total length $L_t$ (μm) as function of resonance frequency for several values of $W$ (μm) and $\mu_c$ (eV), obtained via FDTD simulations.
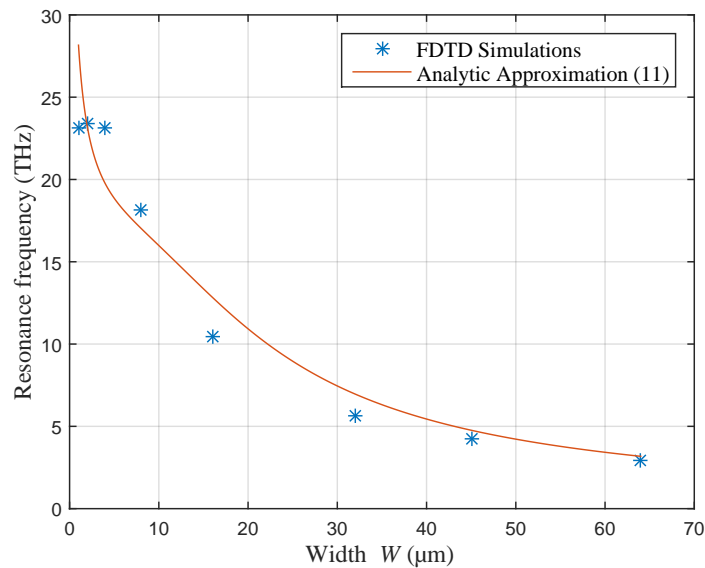
*Brazilian Microwave and Optoelectronics Society-SBMO*     *received 8 May 2021; for review 17 May 2021; accepted 6 Nov 2021*

*Brazilian Society of Electromagnetism-SBMag*     *© 2022 SBMO/SBMag*     (cc) BY     *ISSN 2179-1074*

Fig. 4. Resonance frequency of the metallic dipole antenna (no graphene sheets), with $L_t = L_s = 3$ μm, obtained using FDTD simulations and the analytic approximation (11).

is the complete elliptic integral of the first kind [52], and

$$k = d_{\text{gap}}/(2d_{\text{metal}} + d_{\text{gap}}), \tag{9}$$

where $d_{\text{gap}} = 2$ μm is the distance between the two plates and $d_{\text{metal}} = 0.5$ μm is the width of the plates (see Fig. 1(b)). These are the same dimensions used in a number of works [16] [22] [27] [29] [35] [39] [53]. Other works use similar source parameters [17] [28] [38] [54], including the paper [55], in which experimental results are shown.

If we consider the metallic electrodes and the source space, the self-inductance of the metallic electrodes is given by [56]

$$L = 2.10^{-9}L_s \left[ \log\left(\frac{2L_s}{W}\right) + 0.5 + 0.2235\frac{W}{L_s} \right], \tag{10}$$

where $L_s$ is the separation between the dipole graphene arms (see Fig. 1(b)). Once (8)−(10) are calculated, the resonance frequency of the metallic dipole antenna (with no graphene sheets) can be approximated by using the well-known LC circuit equation

$$f_{\text{m}} = \frac{1}{2\pi\sqrt{LC}}. \tag{11}$$

Figure 4 shows that there is a good agreement between the results obtained from (11) and from FDTD simulations for several values of $W$, with $L_t = L_s = 3$ μm.

By once more considering the graphene sheets as part of the structure, the resonance frequency $f_{\text{m}}$ can be used to calculate the phase contribution of the source and metallic parts, overall measuring $L_s$, which is obtained by

$$\theta_{\text{s}} = \pi\frac{f_r}{f_{\text{m}}}, \tag{12}$$

where $f_r$ is the graphene dipole first resonance frequency. Thus, the half-cycle contribution of both

graphene sheets in the dipole antenna is

$$\theta_{\mathrm{g}} = \pi - \theta_{\mathrm{s}}. \tag{13}$$

Finally, the total length of the graphene antenna designed to resonate at $f$ can be calculated by (see Fig. 1)

$$L_{\mathrm{t}} = L_{\mathrm{s}} + L_{\mathrm{g}}, \tag{14}$$

where $L_{\mathrm{s}} = 3$ μm is the source and metallic parts total length and $L_{\mathrm{g}}$ is the total length of the pair of graphene sheets, which can be calculated by

$$L_{\mathrm{g}} = \frac{\theta_{\mathrm{g}}}{\beta}. \tag{15}$$

One should notice that $L_{\mathrm{t}}$ will depend on the surface plasmonic phase constant $\beta$, of which calculation approach is detailed in the next section. A concise algorithm developed for calculating $L_{\mathrm{t}}$ is given in the Appendix.

## IV. CALCULATION OF PLASMONIC PHASE CONSTANT $\beta$

If we assume that the width of the graphene strip is much smaller than the plasmonic wavelength, i.e. $W \ll \lambda_{spp}$, the surface plasmons will have a quasi-electrostatic nature [45]. This property allows the calculation of the phase constant $\beta$ by using a scaling law [45] [46]. Under the mentioned circumstances, the quasi-electrostatic scaling parameter $\eta_{\mathrm{qes}}$ is given by

$$\eta_{\mathrm{qes}} = \frac{\mathrm{Im}[\sigma(f_{\beta})]}{f_{\beta} W \varepsilon_{\mathrm{eff}}}, \tag{16}$$

where $\sigma(f_{\beta})$ is the graphene surface conductivity at frequency $f_{\beta}$ (frequency of plasmon wave regarding phase constant $\beta$), and $\varepsilon_{\mathrm{eff}}$ is the effective permittivity. The scaling law enables the scaling parameter $\eta_{\mathrm{qes}}$ to be approximated by a function depending on the product $\beta W$ [45] [46]. Aiming at validation, full-wave simulations were performed in [46] for different graphene strip configurations, confirming that, since $W \ll \lambda_{spp}$, the function $\eta_{\mathrm{qes}}(\beta W)$ is unchanged.

In this work, graphene ribbons widths range from 1 to 32 μm, which can be comparable to $\lambda_{spp}$ in the THz range and, thus, the behavior of surface plasmons is not compatible with quasi-electrostatic physics. However, under this circumstance, a correction factor can be defined in order to make the employment of the scaling law feasible. This paper does not cover THz antennas with widths larger than 32 μm because these devices tend to concentrate the surface current distribution on the borders of the graphene sheets, as can be noticed in Fig. 5, intricating the use of the scaling law at the antennas' resonance frequency.

In order to calculate the function $\eta(\beta W)$ for the graphene strips in each antenna studied in this work, the scaling parameter $\eta$ is calculated by using the graphene dipole first resonance frequency $f_{r}$, which is obtained by running an FDTD simulation. Thus, once $f_{r}$ is known, we compute

$$\eta = \frac{\mathrm{Im}[\sigma(f_{r})]}{f_{r} W \varepsilon_{\mathrm{eff}}}, \tag{17}$$

and plot results as a function of $\beta W$, where the phase constant $\beta$ is determined by rearranging (15) as
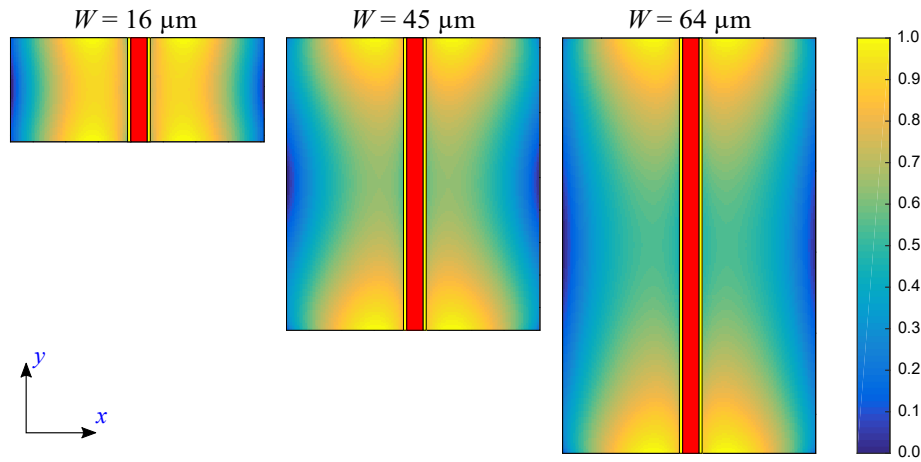
$$\beta = \frac{\theta_{\mathrm{g}}}{L_{\mathrm{g}}}. \tag{18}$$

Fig. 5. Normalized magnitude of the surface current distribution for graphene dipole antennas with $\mu_c = 0.1$ eV, $L_t = 39$ μm and width equal to $W = 16$ μm, 32 μm and 64 μm.

The function $\eta(\beta W)$ for the graphene dipoles over the glass substrate, for various levels of the graphene chemical potential $\mu_c$, can be seen in Fig. 6 along with the quasi-static curve $\eta_{qes}$. As it can be seen in Fig. 6, for the cases studied in this paper, differences between $\eta$ and $\eta_{qes}$ cannot be disregarded. Since FDTD is a full-wave method, all wave effects are taken into account, including those associated with the coupling fields among the structure parts, the fringing fields around the antennas' edges, and wave reflections and refractions associated with the substrate.

Considering the log-log scale used to plot the data in Fig. 6, the values computed for $\eta$ can be approximated by a straight line depending on the parameters $\mu_c$ and $W$, i.e,

$$\log_e(\beta \times W) \approx a \log_e \eta + b, \tag{19}$$

in which $a$ and $b$ are functions of $W$ and $\mu_c$. The parameters $a$ and $b$, which can be seen graphically in Fig. 7, are obtained by using the Least Square Method (LSM) [57] as functions of $W$ and $\mu_c$. The functions $a$ and $b$ were approximated by the rational equations, given respectively by

$$a \approx \frac{p_{1a} \cdot \mu_c + p_{2a}}{\mu_c + q_a} \tag{20}$$

and

$$b \approx \frac{p_{1b} \cdot \mu_c + p_{2b}}{\mu_c + q_b}, \tag{21}$$

where $p_{1a}$, $p_{2a}$, $q_a$, $p_{1b}$, $p_{2b}$, and $q_b$ are functions of the width $W$ obtained once more by employing LSM over FDTD data. The obtained samples of the parameters in (20) and (21) are shown in Fig. 8 along with their respective fitting rational equations given by

$$p_{1a} \approx \frac{5178W^2 - 0.6532W - 2.959 \times 10^{-6}}{W + 5.49 \times 10^{-6}}, \tag{22}$$

$$p_{2a} \approx \frac{-5605W^2 - 0.1129 + 3.613 \times 10^{-9}}{W - 4.066 \times 10^{-7}}, \tag{23}$$

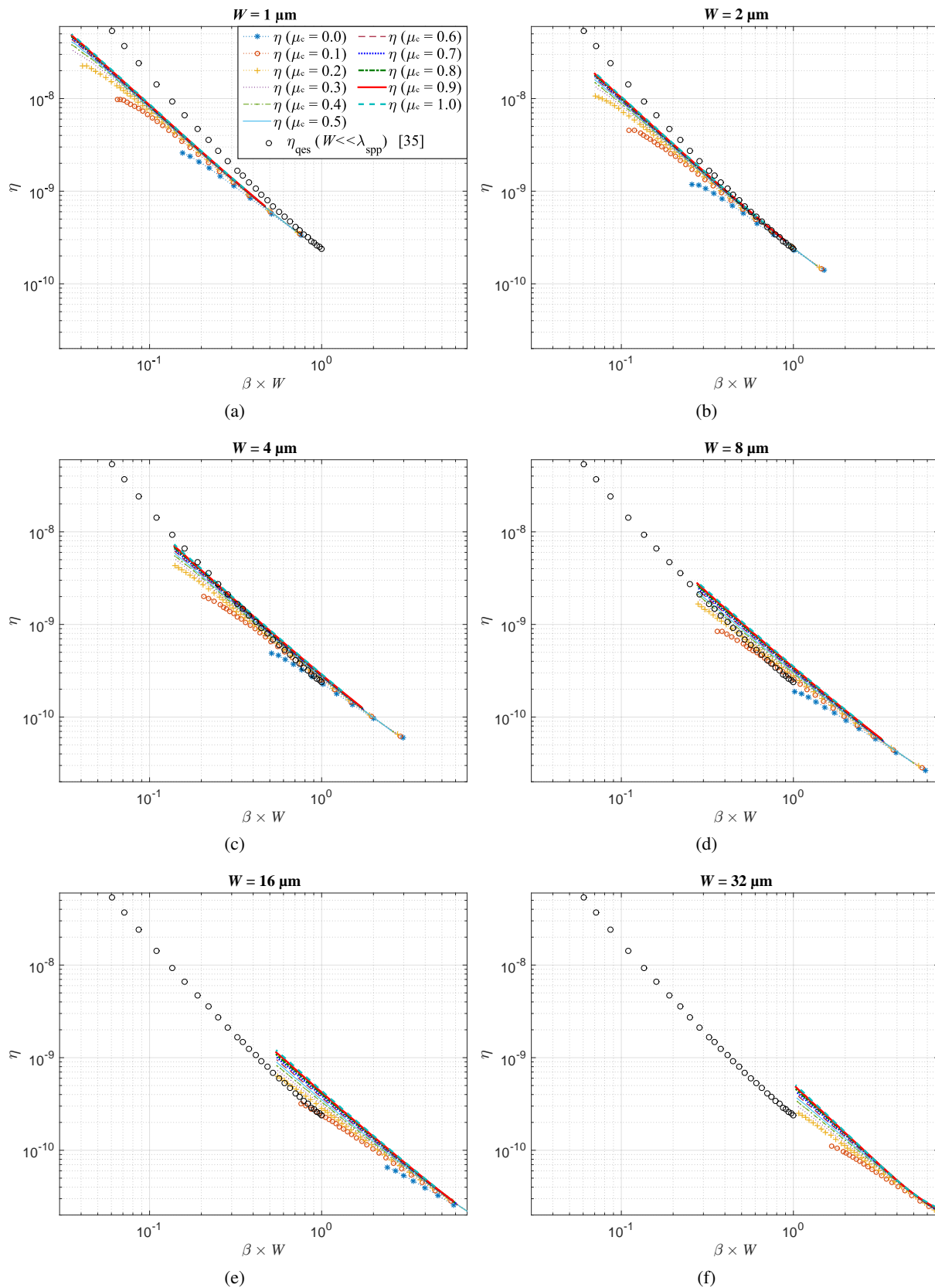$$q_a \approx \frac{5327W^2 + 0.1349W + 5.036 \times 10^{-8}}{W - 2.507 \times 10^{-7}}, \tag{24}$$

Fig. 6. The parameter $\eta$ calculated using FDTD simulations considering several values of $W$ and $\mu_c$ ($\lambda_{spp}$ is comparable to $W$), along with $\eta_{qes}$ (represented by white circles, in which $W \ll \lambda_{spp}$).
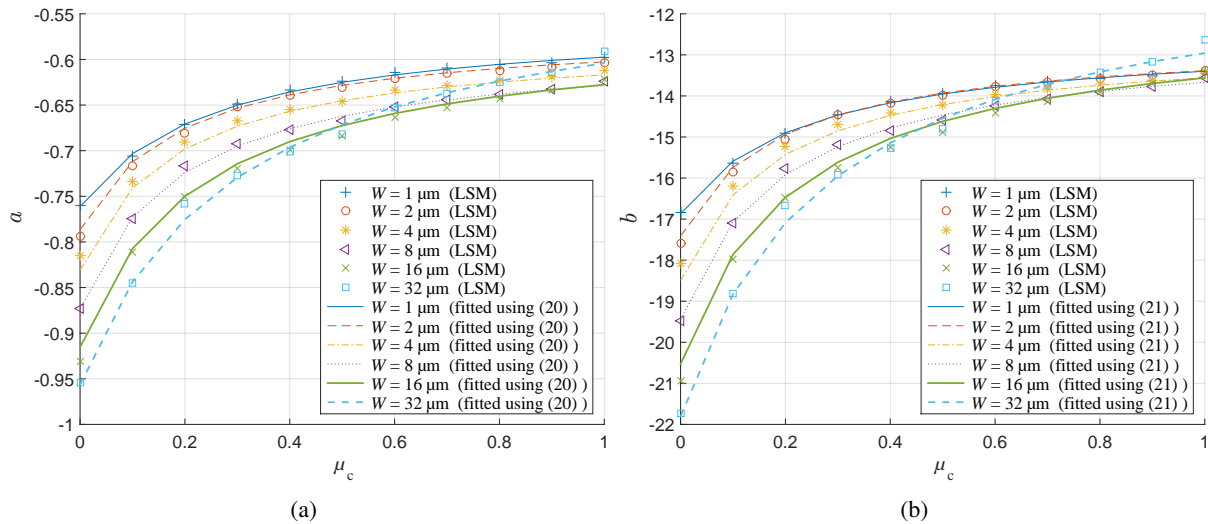
Fig. 7. The parameters (a) $a$ and (b) $b$, obtained by using the Least Squares Method, and their respective fitting curves.

$$p_{1b} \approx \frac{1.233 \times 10^5 \times W^2 - 13.66W - 0.0001501}{W + 1.2 \times 10^{-5}}, \tag{25}$$

$$p_{2b} \approx \frac{-1.021 \times 10^5 \times W^2 - 2.755W + 1.906 \times 10^{-6}}{W - 7.594 \times 10^{-7}} \tag{26}$$

and

$$q_b \approx \frac{3933W^2 + 0.151W - 4.389 \times 10^{-8}}{W - 5.262 \times 10^{-7}}, \tag{27}$$

where the constants in (22)-(27) were computed once more by using the LSM. In this work, all the LSM fits were performed by using the Matlab platform.

Once all parameters are properly fitted, it is possible to plot the approximating curves for $\eta$, as it can be seen in Fig. 9. Finally, the phase constant is obtained by using (19), which produces

$$\beta \approx \frac{\eta^a \times e^b}{W}. \tag{28}$$

When Figs. 6 and 9 are compared, one can see that the proposed formulas can, in fact, properly predict $\eta$. In order to obtain an approximation $L_{eq}$ for $L_t$, one must calculate: the capacitance between metallic electrodes using (8), the self-inductance of electrodes with (10), the resonance of metallic electrodes by employing (11), the phase associated with graphene sheets with (13), the graphene conductivity $\sigma$ using (1), the scaling parameter given by (17), the parameters $a$ and $b$ with (20) and (21), respectively, the phase constant $\beta$ using (28), the total length of graphene sheets using (15) and, finally, the estimate $L_{eq}$ is given by (14). An algorithm developed for calculating $L_{eq}$ is given in the Appendix. The accuracy of the proposed formulation is calculated and discussed in the following section.

## V. ACCURACY OF THE PROPOSED FORMULATION

In this section, the accuracy of the proposed formulation developed for estimating $L_t$ using the algorithm in the Appendix for calculating $L_{eq}$ is measured. Figure 10 shows the estimate $L_{eq}$ (approximation of graphene dipole antenna length $L_t$), as a function of dipole resonance frequency, calculated by employing the proposed formulation for several values of $W$ and $\mu_c$. Initially, in a qualitative perspective,
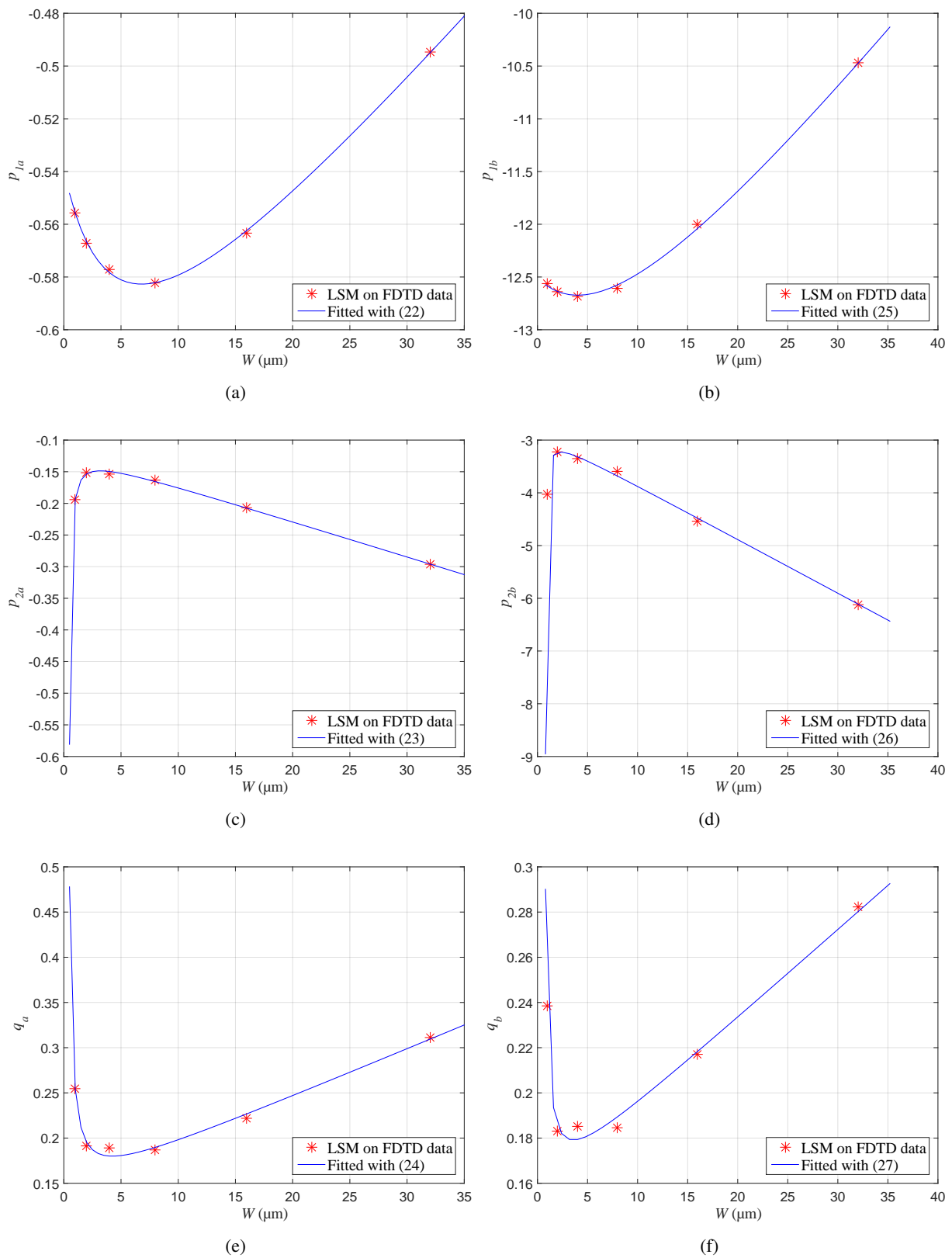
Fig. 8. The parameters (a) $p_{1a}$, (b) $p_{1b}$, (c) $p_{2a}$, (d) $p_{2b}$, (e) $q_a$ and (f) $q_b$ obtained with LSM applied over FDTD data and their respective fitting curves.

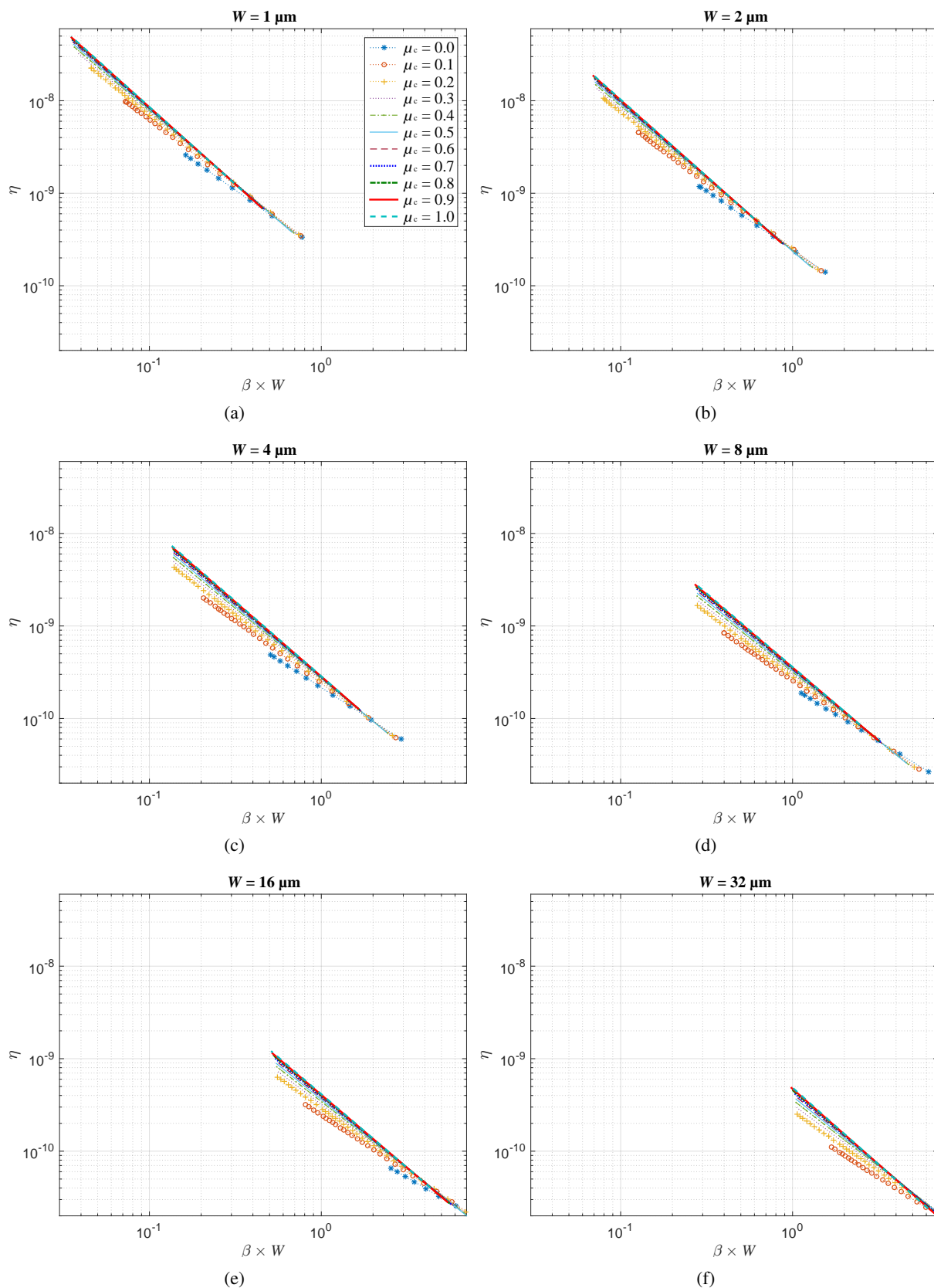*Brazilian Microwave and Optoelectronics Society-SBMO*       *received 8 May 2021; for review 17 May 2021; accepted 6 Nov 2021*

*Brazilian Society of Electromagnetism-SBMag*       *© 2022 SBMO/SBMag*       (cc) BY       *ISSN 2179-1074*

Fig. 9. Approximations for $\eta$ calculated using (19) and several values of $W$ and $\mu_c$.

one notices that curves in Figs. 10 and 3 are comparable, showing similar general behaviors.

Figure 11 indicates the ratio $L_{eq}/L_t$, which, in cases of perfect approximations, should be equal to one. For $W = 1$ μm and $W = 2$ μm, the obtained ratios are the closest to one, ranging between 0.978 and 1.029), except for the frequencies lower than 0.4 THz. Deviations from unitary $L_{eq}/L_t$ ratios start to increase as $W$ is increased from 4 μm on. Additionally, there is a clear tendency of the ratio to grow away from 1 at higher frequencies, particularly above 3 THz. However, the maximum obtained relative absolute error is 6.77% if 3 THz is the maximum considered frequency.

In order to measure the average accuracy of the proposed formulation, the mean relative absolute error is calculated, which is given by

$$\text{MRAE} = \frac{1}{N} \sum_{i=1}^{N} \frac{|L_{eq}(i) - L_t(i)|}{L_t(i)} \times 100\%, \tag{29}$$

where $N = 2178$ is the total number of FDTD simulations in which all the considered variations of parameters are taken into account. For the frequency range of data shown in Fig. 11 (from 0.3 THz to 3.8 THz), MRAE is equal to 1.63% (with a maximum relative absolute error of 12.44%). The higher values of relative absolute error are obtained at the lowest and the highest frequencies of the analyzed band, i.e., 0.3 THz and 3.8 THz, respectively, as previously discussed. When considering the use of the proposed formulation in the frequency range from 0.5 THz to 3.0 THz, the relative mean absolute error is reduced to 1.50%, while the maximum relative absolute error is diminished to 6.77%. The deviation levels obtained between 0.5 THz to 3.0 THz is acceptable from engineering and numerical points of view. The formulation can be used for fast calculation of the length of the graphene dipole antenna, with no need for intense computational full-wave simulations.

## VI. IMPEDANCE MATCHING

In order to maximize the radiation efficiency, we studied the resistance value of the input impedance $R = \text{Re}\{Z\}$ at the dipole first resonance frequency, when $Z$ is purely real. By using the results of the FDTD simulations in this work, we can plot this resistance curve of the antennas as a function of the length as seen in Fig. 12. The curves indicate that the input resistance at the first resonance frequency increases almost linearly with the increase of the antenna length. Moreover, smaller values of $\mu_c$ result in bigger increase coefficient, while the increase of $W$ decreases the input resistance.

In this work, we approximated the input resistance curve $R$ by a straight line depending on the parameters $\mu_c$ and $W$, i.e,

$$R \approx A \times L + B, \tag{30}$$

in which $A$ and $B$ are functions of $W$ and $\mu_c$. By a similar fitting process executed in Section IV, we used the LSM to approximate the $A$ and $B$ parameters with rational equations, given respectively by

$$A \approx 10^8 \times \frac{p_{1A}.\mu_c^2 + p_{2A}.\mu_c + p_{3A}}{q_A.\mu_c + 14.\mu_c + 1} \tag{31}$$

and

$$B \approx \frac{p_{1B}.\mu_c + p_{2B}}{q_{1B}.\mu_c^2 + q_{2B}.\mu_c + 1}, \tag{32}$$

where $p_{1A}$, $p_{2A}$, $p_{3A}$, $q_A$, $p_{1B}$, $q_{1B}$, $p_{2B}$, and $q_{2B}$ are functions of the width $W$ obtained once more
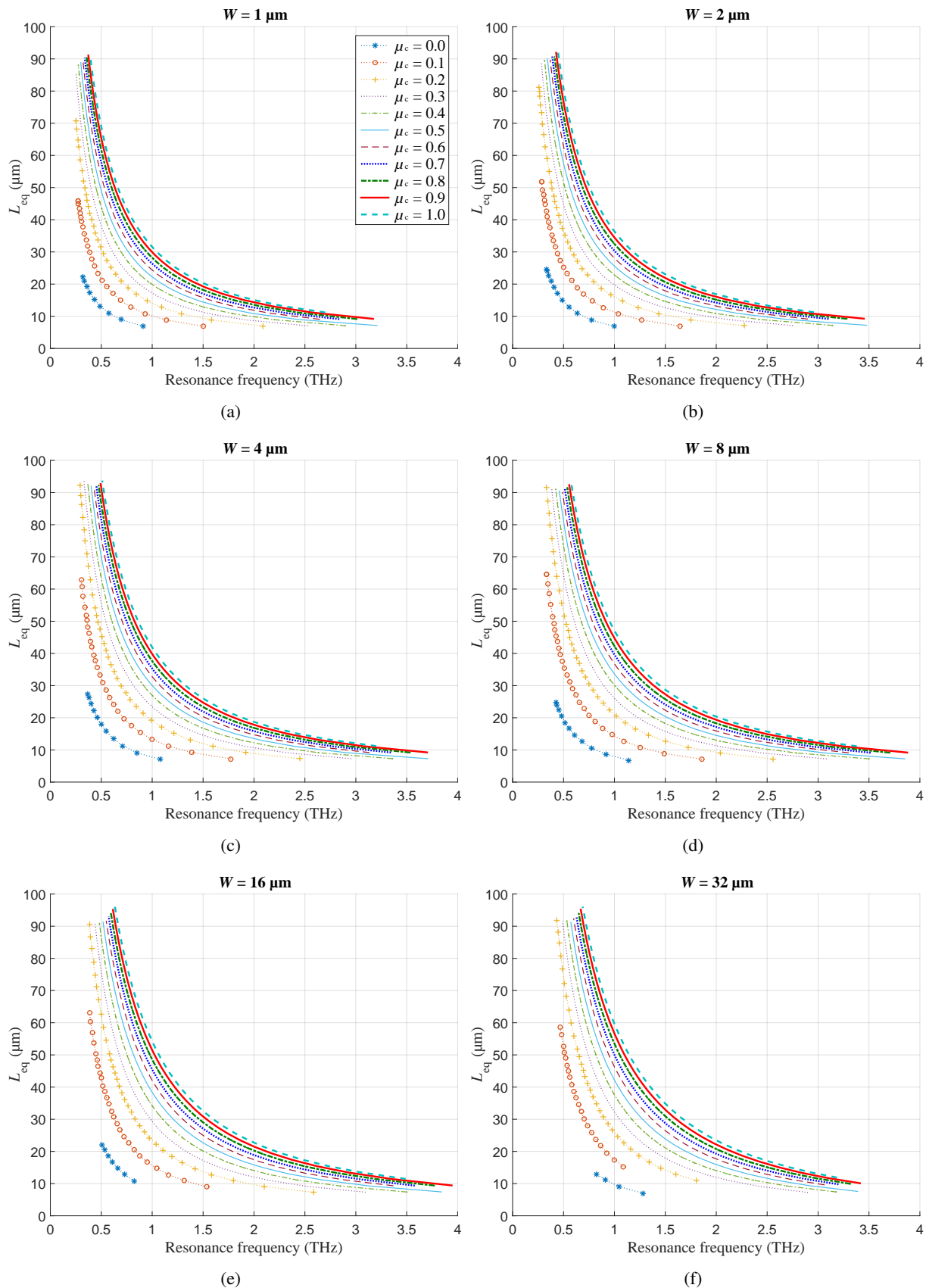
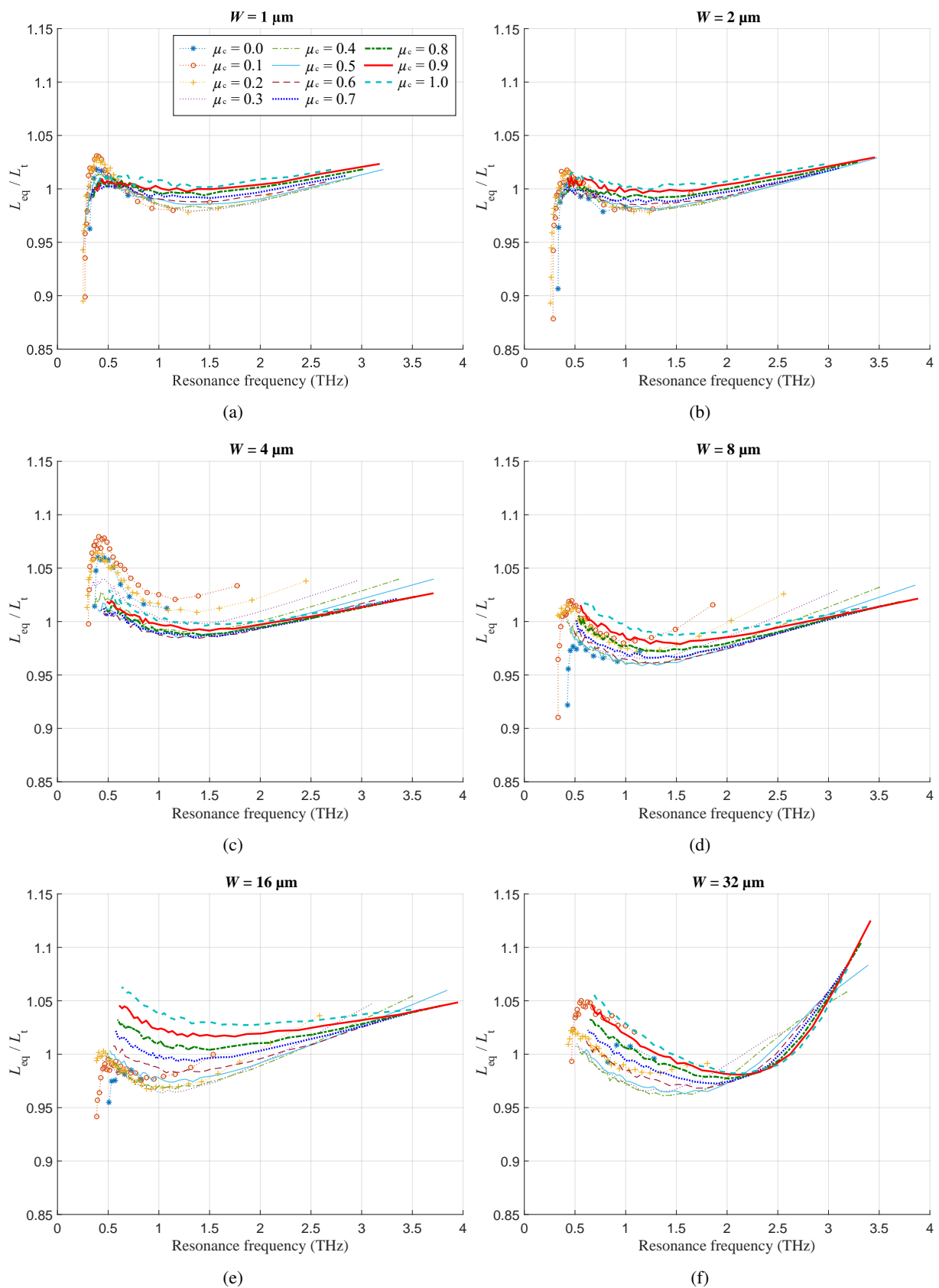Fig. 10. $L_{eq}$ calculated using (14) as functions of the resonance frequency for several values of $W$ and $\mu_c$.

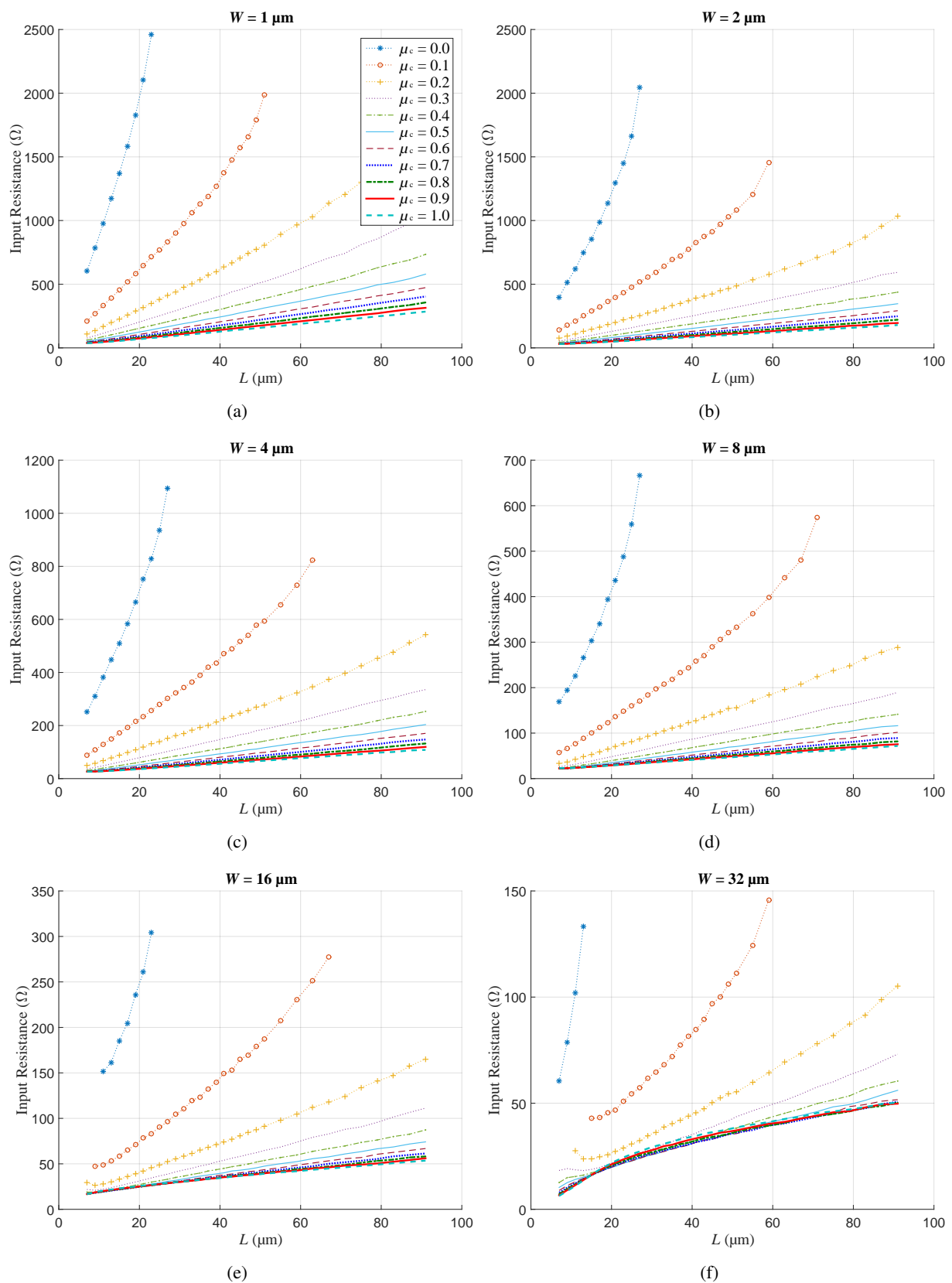Fig. 11. Ratios $L_{eq}/L_t$ as functions of resonance frequency, for several values of $W$ and $\mu_c$ (eV).

Fig. 12. Input Resistance $R = \mathrm{Re}\{Z\}$ at the dipole first resonance frequency as functions of the antenna's length $L$, for several values of $W$ and $\mu_c$ (eV).

by employing LSM given by

$$
\begin{aligned}
p_{1A} \approx\ & 0.85 + 520.5 e^{(-8.446 \times 10^{-5} \times W)} \sin(8.387 \times 10^3 \times W - 8.241 \times 10^{-3}) \\
& + 7.6750 \times 10^{-4} \times e^{(2.951 \times 10^5 \times (W - 1.5 \times 10^{-5}))} - 1,
\end{aligned}
\tag{33}
$$

$$
p_{2A} \approx \frac{0.92 W^3 + 0.3585 W^2 - 1589 W + 0.1717}{1.764 \times 10^4 \times W + 0.001},
\tag{34}
$$

$$
p_{3A} \approx \begin{cases} 9.349 \times 10^{10} \times W^2 - 8.347 \times 10^5 \times W + 2.379, & W < 4\mu\text{m} \\ 0.767 e^{(-1.597 \times 10^5 \times W)} + 0.1354 e^{(-9106 * W)}, & \text{else} \end{cases},
\tag{35}
$$

$$
q_A \approx -9.229 \times 10^5 \times W + 375.1,
\tag{36}
$$

$$
p_{1B} \approx \frac{2710}{1.875 \times 10^5 \times W + 1},
\tag{37}
$$

$$
p_{2B} \approx \begin{cases} 3.984 \times 10^{13} \times W^2 + 8.771 \times 10^7 \times W - 1334, & W < 4\mu\text{m} \\ \frac{-6.57 \times 10^{11} \times W^2 + 3.444 \times 10^7 \times W - 432.1}{-2.963 \times 10^4 \times W + 1}, & \text{else} \end{cases},
\tag{38}
$$

$$
q_{1B} \approx \frac{-5.908 \times 10^{16} \times W^3 + 1.488 \times 10^{11} \times W^2 + 1.067 \times 10^7 \times W + 30.27}{1.745 \times 10^{11} \times W^2 - 6.153 \times 10^5 \times W + 1}
\tag{39}
$$

and

$$
q_{2B} \approx \frac{8.229 \times 10^{11} \times W^2 + -8.772 \times 10^7 \times W + 62.19}{-2.312 \times 10^6 \times W + 1}.
\tag{40}
$$

A concise algorithm developed for calculating $R$ is given in the Appendix.

The accuracy of this formulation is calculated by the mean relative absolute error, which is given by

$$
\text{MRAE} = \frac{1}{N} \sum_{i=1}^{N} \frac{|R_{\text{eq}}(i) - R_{\text{t}}(i)|}{R_{\text{t}}(i)} \times 100\%,
\tag{41}
$$

where $N = 2178$ is the total number of FDTD simulations. The MRAE is equal to 6.09%, with a maximum relative absolute error of 228,57%. High values of relative absolute error are due to the smaller dipole length (i.e., $L < 25$ μm) and smaller chemical potential values (i.e., $\mu_{\text{c}} < 0.2$ eV), where the input resistance increase is less linear as a function of the dipole length, as can been seen in Fig. 12. When considering the use of the proposed formulation in the dipole length range from 25 to 91 μm and chemical potential from 0.2 to 1.0 eV, the relative mean absolute error is reduced to 1.94%, while the maximum relative absolute error is diminished to 7.38%. This way, the formulation becomes applicable from the engineering and numerical perspectives.

The input resistance of the graphene dipole can be matched to the internal resistance of the photomixer proposed in [48], which has a graphene-based emitter. By adjusting its internal Fermi energy $\mu_{\text{ce}}$ and considering its physical dimensions, the internal resistance of the photomixer is given by

$$
Z_0 = \sqrt{\frac{R_{\text{S}} + j\omega (L_{\text{K}} + L_{\text{m}})}{j\omega C_{\text{es}}}},
\tag{42}
$$

where

$$
R_{\text{S}} = \frac{2\text{Re}\{1/\sigma\}}{W}
$$

TABLE I. PHOTOMIXER PARAMETERS FOR IMPEDANCE MATCHING WITH THE DIPOLE ANTENNA

| Antenna parameters | | | Photomixer parameters | | |
|---|---|---|---|---|---|
| $W$ | $\mathrm{Re}\{Z\}_{\min}$ | $\mathrm{Re}\{Z\}_{\max}$ | $d$ | $Z_{0\min}$ ($\mu_{ce}=1$ eV) | $Z_{0\max}$ ($\mu_{ce}=0$) |
| 1 μm | 50 Ω | 2500 Ω | 1.06 μm | 491.9 Ω | 2505.7 Ω |
|  |  |  | 0.2 nm | 9.92 Ω | 52.4 Ω |
| 2 μm | 50 Ω | 2100 Ω | 4.5 μm | 467.2 Ω | 2150.5 Ω |
|  |  |  | 0.8 nm | 9.92 Ω | 52.3 Ω |
| 4 μm | 50 Ω | 1100 Ω | 2.8 μm | 231.1 Ω | 1115 Ω |
|  |  |  | 3 nm | 9.6 Ω | 50.3 Ω |
| 8 μm | 50 Ω | 700 Ω | 3.9 μm | 150.8 Ω | 705.2 Ω |
|  |  |  | 12 nm | 9.6 Ω | 50.7 Ω |
| 16 μm | 30 Ω | 310 Ω | 2.2 μm | 63.4 Ω | 311.3 Ω |
|  |  |  | 50 nm | 9.8 Ω | 51.6 Ω |
| 32 μm | 10 Ω | 150 Ω | 1.9 μm | 30.8 Ω | 152.5 Ω |
|  |  |  | 190 nm | 9.6 Ω | 50.2 Ω |

TABLE II. RADIATION EFFICIENCY VALUES FOR GRAPHENE DIPOLE ANTENNA WITH $L_T = 41$ μM AND $\mu_c = 1$ EV AT ITS RESPECTIVE FIRST RESONANCE FREQUENCY $f_1$.

| $W$ | $f_1$ | Radiation efficiency |
|---|---|---|
| 2 μm | 0.9 THz | 16.05% |
| 8 μm | 1.1 THz | 52.45% |
| 32 μm | 1.3 THz | 79.52% |

is the sheet resistance,

$$L_K = \frac{2\mathrm{Im}\{1/\sigma\}}{\omega W}$$

is the kinetic inductance,

$$L_m = \mu_0 \frac{d_p}{W}$$

is the magnetic inductance and

$$C_{es} = \varepsilon_{ox}\varepsilon_0 \frac{W}{d_p} + \varepsilon_{ox}\varepsilon_0 \frac{\pi}{\log_e[6(d_p/W + 1)]}$$

is due to the parallel-plate capacitance between the two graphene sheets used in the photomixer, such as described in [48]. Based on the resistance values depicted in Fig. 12 for each width $W$, the parameters $\mu_{ce}$ and $d_p$ that lead to impedance matching with the graphene antenna are indicated in Table I, in which $d_p$ is the distance between the graphene parallel-plate waveguides in the photomixer [48]. Therefore, the implementation of the graphene device proposed in this paper is feasible, with radiation efficiency values expected to be between 10% and 80%, such as indicated in Table II for the graphene dipole antenna with $L_t = 41$ μm at its respective first resonance frequency $f_1$ for $\mu_c = 1$ eV and $W$ equal to 2 μm, 8 μm, and 32 μm.

## VII. FINAL REMARKS

In this paper, a semi-analytical formulation is developed for fast calculation of the total length of graphene dipole antennas, since width, chemical potential, and desired resonance frequency are given. First resonance frequencies of rectangular graphene dipole antennas laying on glass substrate

are obtained by using the FDTD method. From the obtained numerical results and with the use of the Least Square Method, the proposed formulation is developed.

In order to measure the accuracy of the proposed formulation, the mean relative absolute error (MRAE) is calculated. For the frequency range between 0.5 and 3.0 THz, MRAE = 1.5%, while the maximum relative absolute error, obtained at the ends of the frequency range, is 6.77%.

The lengths of graphene dipole antennas can be calculated instantaneously by using a very simple proposed algorithm, with the advantage of no need for computationally intense full-wave electrodynamics simulations. Other important advantages are that the proposed formulation supports finite-width graphene dipoles and it takes into account the relevant influence of photomixer sources. THz telecommunication engineers can benefit from fast design possibilities provided by the proposed algorithm, which support a very large number of combinations of geometrical and electrical parameters.

To obtain maximum radiation efficiency, we studied the input resistance at resonance for the different antenna settings. These resistance results were fitted with LSM with an accuracy of MRAE = 1.94% for the range $25 \leq L_\mathrm{t} \leq 91\mu\mathrm{m}$ and $0.2 \leq \mu_\mathrm{c} \leq 1.0$, while the maximum relative absolute error is 7.38%. By using a graphene-based emitter photomixer for input resistance matching, we conclude that the antenna is feasible, with radiation efficiency values up till 80%.

APPENDIX

---

**ALGORITHM 1:** Calculation of the total length of the graphene dipole.

**Input** : fr – resonance frequency, float between 0.5e+12 and 3e+12 (Hz)
W – graphene dipole width, float between 1e-6 and 32e-6 (m)
μc – chemical potential, float between 0.0 and 1.0 (eV)

**Output:** Leq – estimate of graphene dipole total length Lt (m)

```
1  C  ← ε_eff W × ellipke(√(1−k²))/ellipke(k)     /* capacitance due the metallic electrodes (8) */
2  Ls ← 3e-6                                        /* source + metallic parts length */
3  L  ← 2e-9Ls[log(2Ls/W) + 0.5 + 0.2235 W/Ls]     /* self-inductance of the metallic electrodes (10) */
4  fm ← 1/(2π√(L × C))                              /* resonance frequency of the metallic electrodes (11) */
5  θg ← π(1 − fr/fm)                                /* phase associated to graphene sheets (13) */
6  σ  ← kubo(2π × fr)                               /* graphene patch conductivity (Kubo's formula) (1) */
7  η  ← Im(σ)/(fr × W × ε_eff)                      /* scaling parameter (17) */
8  a  ← calca(μc, W)                                /* calculates the parameter 'a' (20) */
9  b  ← calcb(μc, W)                                /* calculates the parameter 'b' (21) */
10 β  ← η^a × e^b/W                                 /* phase constant (28) */
11 Lg ← θg/β                                        /* total length of the pair of graphene sheets (15) */
12 Leq ← Ls + Lg                                    /* total length of the graphene dipole antenna (14) */
```

---

**ALGORITHM 2:** Calculation of the input resistance at resonance frequency of the graphene dipole.

**Input** : L – antenna length, float between 7e-6 and 91e-6 (m)
W – graphene dipole width, float between 1e-6 and 32e-6 (m)
μc – chemical potential, float between 0.0 and 1.0 (eV)

**Output:** Req – estimate of input resistance R (Ω)

```
1  A  ← calcA(μc, W)                                /* calculates the parameter 'A' (31) */
2  B  ← calcB(μc, W)                                /* calculates the parameter 'B' (32) */
3  Req ← A × L + B                                  /* input resistence of the graphene dipole antenna (30) */
```

---

ACKNOWLEDGMENTS

REFERENCES

[1] A. K. Geim and K. S. Novoselov, "The rise of graphene," in *Nanoscience and Technology: A Collection of Reviews from Nature Journals*. World Scientific, 2010, pp. 11–19.

[2] K. S. Novoselov, A. K. Geim, S. V. Morozov, D. Jiang, Y. Zhang, S. V. Dubonos, I. V. Grigorieva, and A. A. Firsov, "Electric field effect in atomically thin carbon films," *Science*, vol. 306, no. 5696, pp. 666–669, 2004.

[3] S. K. Tiwari, S. Sahoo, N. Wang, and A. Huczko, "Graphene research and their outputs: Status and prospect," *Journal of Science: Advanced Materials and Devices*, vol. 5, no. 1, pp. 10 – 29, 2020.

[4] K. S. Novoselov, V. Fal, L. Colombo, P. Gellert, M. Schwab, K. Kim, *et al.*, "A roadmap for graphene," *Nature*, vol. 490, no. 7419, pp. 192–200, 2012.

[5] R. Wang, X.-G. Ren, Z. Yan, L.-J. Jiang, W. E. I. Sha, and G.-C. Shan, "Graphene based functional devices: A short review," *Frontiers of Physics*, vol. 14, p. 13603, 2019.

[6] M. Jablan, H. Buljan, and M. Soljačić, "Plasmonics in graphene at infrared frequencies," *Physical Review B*, vol. 80, no. 24, p. 245435, 2009.

[7] A. Y. Nikitin, F. Guinea, F. García-Vidal, and L. Martín-Moreno, "Edge and waveguide terahertz surface plasmon modes in graphene microribbons," *Physical Review B*, vol. 84, no. 16, p. 161407, 2011.

[8] I. Llatser, C. Kremers, A. Cabellos-Aparicio, E. Alarcón, D. N. Chigrin, and D. N. Chigrin, "Comparison of the resonant frequency in graphene and metallic nano-antennas," in *AIP Conference Proceedings*, vol. 1475, no. 1, pp. 143–145, 2012.

[9] K. Sengupta, T. Nagatsuma, and D. M. Mittleman, "Terahertz integrated electronic and hybrid electronic–photonic systems," *Nature Electronics*, vol. 1, no. 12, pp. 622–635, 2018.

[10] S. Abadal, C. Han, and J. M. Jornet, "Wave propagation and channel modeling in chip-scale wireless communications: A survey from millimeter-wave to terahertz and optics," *IEEE Access*, vol. 8, pp. 278–293, 2019.

[11] D. Correas-Serrano and J. S. Gomez-Diaz, "Graphene-based antennas for terahertz systems: A review," *arXiv preprint arXiv:1704.00371*, 2017.

[12] G. W. Hanson, "Dyadic Green's functions and guided surface waves for a surface conductivity model of graphene," *Journal of Applied Physics*, vol. 103, no. 6, p. 064302, 2008.

[13] J. S. Gómez-Díaz and J. Perruisseau-Carrier, "Graphene-based plasmonic switches at near infrared frequencies," *Opt. Express*, vol. 21, no. 13, pp. 15 490–15 504, Jul 2013. [Online]. Available: http://www.osapublishing.org/oe/abstract.cfm?URI=oe-21-13-15490

[14] G. J. Adekoya, R. E. Sadiku, and S. S. Ray, "Nanocomposites of PEDOT:PSS with Graphene and its Derivatives for Flexible Electronic Applications: A Review," *Macromolecular Materials and Engineering*, vol. 306, no. 3, p. 2000716, 2021. [Online]. Available: https://onlinelibrary.wiley.com/doi/abs/10.1002/mame.202000716

[15] I. Llatser, C. Kremers, A. Cabellos-Aparicio, J. M. Jornet, E. Alarcón, and D. N. Chigrin, "Graphene-based nano-patch antenna for terahertz radiation," *Photonics and Nanostructures-Fundamentals and Applications*, vol. 10, no. 4, pp. 353–358, 2012.

[16] M. Tamagnone, J. Gomez-Diaz, J. Mosig, and J. Perruisseau-Carrier, "Analysis and design of terahertz antennas based on plasmonic resonant graphene sheets," *Journal of Applied Physics*, vol. 112, no. 11, p. 114915, 2012.

[17] S. K. Tripathi, M. Kumar, and A. Kumar, "Graphene based tunable and wideband terahertz antenna for wireless network communication," *Wireless Networks*, vol. 25, no. 7, pp. 4371–4381, 2019.

[18] J. M. Jornet and I. F. Akyildiz, "Graphene-based nano-antennas for electromagnetic nanocommunications in the terahertz band," in *Proceedings of the Fourth European Conference on Antennas and Propagation*, pp. 1–5, 2010.

[19] I. L. Martí, C. Kremers, A. Cabellos-Aparicio, J. M. Jornet, E. Alarcón, and D. N. Chigrin, "Scattering of terahertz radiation on a graphene-based nano-antenna," in *AIP Conference Proceedings*, vol. 1398, no. 1, pp. 144–146, 2011.

[20] K. Costa, V. Dmitriev, C. Nascimento, and G. Silvano, "Graphene nanoantennas with different shapes," in *2013 SBMO/IEEE MTT-S International Microwave & Optoelectronics Conference (IMOC)*, pp. 1–5, 2013.

[21] I. Llatser, C. Kremers, D. N. Chigrin, J. M. Jornet, M. C. Lemme, A. Cabellos-Aparicio, and E. Alarcón, "Characterization of graphene-based nano-antennas in the terahertz band," in *2012 6th European Conference on Antennas and Propagation (EUCAP)*, pp. 194–198, 2012.

[22] R. M. S. de Oliveira, N. R. Rodrigues, and V. Dmitriev, "FDTD formulation for graphene modeling based on piecewise linear recursive convolution and thin material sheets techniques," *IEEE Antennas and Wireless Propagation Letters*, vol. 14, pp. 767–770, 2015.

[23] D. F. Kelley and R. J. Luebbers, "Piecewise linear recursive convolution for dispersive media using FDTD," *IEEE Transactions on Antennas and Propagation*, vol. 44, no. 6, pp. 792–797, 1996.

[24] J. G. Maloney and G. S. Smith, "The efficient modeling of thin material sheets in the finite-difference time-domain (FDTD) method," *IEEE Transactions on antennas and Propagation*, vol. 40, no. 3, pp. 323–330, 1992.

[25] J. T. Bernhard, "Reconfigurable antennas," *Synthesis Lectures on Antennas*, vol. 2, no. 1, pp. 1–66, 2007.

[26] N. R. N. M. Rodrigues, R. M. S. de Oliveira, and V. Dmitriev, "Smart terahertz graphene antenna: Operation as an omnidirectional dipole and as a reconfigurable directive antenna," *IEEE Antennas and Propagation Magazine*, vol. 60, no. 5, pp. 26–40, 2018.

[27] M. Tamagnone, J. Gomez-Diaz, J. R. Mosig, and J. Perruisseau-Carrier, "Reconfigurable terahertz plasmonic antenna concept using a graphene stack," *Applied Physics Letters*, vol. 101, no. 21, p. 214102, 2012.

[28] T. Zhou, Z. Cheng, H. Zhang, M. Berre, L. Militaru, and F. Calmon, "Miniaturized tunable terahertz antenna based on graphene," *Microwave and Optical Technology Letters*, vol. 56, no. 8, pp. 1792–1794, 2014.

[29] M. Tamagnone and J. Perruisseau-Carrier, "Predicting input impedance and efficiency of graphene reconfigurable dipoles using a simple circuit model," *IEEE Antennas and Wireless Propagation Letters*, vol. 13, pp. 313–316, 2014.

[30] A. Cabellos-Aparicio, I. Llatser, E. Alarcon, A. Hsu, and T. Palacios, "Use of terahertz photoconductive sources to characterize tunable graphene RF plasmonic antennas," *IEEE Transactions on Nanotechnology*, vol. 14, no. 2, pp. 390–396, 2015.

[31] S. Kumar, D. Parks, and K. Kamrin, "Mechanistic origin of the ultrastrong adhesion between graphene and a-SiO2: beyond van der waals," *ACS nano*, vol. 10, no. 7, pp. 6552–6562, 2016.

[32] P. A. D. Gonçalves and N. M. Peres, *An introduction to graphene plasmonics*. World Scientific, 2016.

[33] Z. Dai, N. Lu, K. M. Liechti, and R. Huang, "Mechanics at the interfaces of 2d materials: Challenges and opportunities," *Current Opinion in Solid State and Materials Science*, vol. 24, no. 4, p. 100837, 2020.

[34] S. Kosuga, R. Suga, O. Hashimoto, and S. Koh, "Graphene-based optically transparent dipole antenna," *Applied Physics Letters*, vol. 110, no. 23, p. 233102, 2017.

[35] B. Zhang, J. Zhang, C. Liu, Z. P. Wu, and D. He, "Equivalent resonant circuit modeling of a graphene-based bowtie antenna," *Electronics*, vol. 7, no. 11, p. 285, 2018.

[36] R. Goyal and D. K. Vishwakarma, "Design of a graphene-based patch antenna on glass substrate for high-speed terahertz communications," *Microwave and Optical Technology Letters*, vol. 60, no. 7, pp. 1594–1600, 2018.

[37] S. Rakheja, P. Sengupta, and S. M. Shakiah, "Design and circuit modeling of graphene plasmonic nanoantennas," *IEEE Access*, vol. 8, pp. 129 562–129 575, 2020.

[38] R. Inum, M. M. Rana, and K. N. Shushama, "Performance analysis of graphene based nano dipole antenna on stacked substrate," in *2016 2nd International Conference on Electrical, Computer & Telecommunication Engineering (ICECTE)*, pp. 1–4, 2016.

[39] M. Aidi, M. Hajji, A. Ben Ammar, and T. Aguili, "Graphene nanoribbon antenna modeling based on MoM-GEC method for electromagnetic nanocommunications in the terahertz range," *Journal of Electromagnetic Waves and Applications*, vol. 30, no. 8, pp. 1032–1048, 2016.

[40] M. Aidi, M. Hajji, H. Messaoudi, and T. Aguili, "Modelling of graphene nanoribbons antenna based on MoM-GEC method to enhance nanocommunications in terahertz range," *Handbook of Graphene, Volume 8: Technology and Innovations*, p. 359, 2019.

[41] J. Perruisseau-Carrier, M. Tamagnone, J. S. Gomez-Diaz, and E. Carrasco, "Graphene antennas: Can integration and reconfigurability compensate for the loss?" in *2013 European Microwave Conference*, pp. 369–372, 2013.

[42] L. Zhang, J. Cai, X. Bian, X. Wu, and J. Feng, "A novel THz forward and backward wave two-mode band-edge oscillator," *IEEE Transactions on Terahertz Science and Technology*, 2020.

[43] Y. S. Cao, L. J. Jiang, and A. E. Ruehli, "An equivalent circuit model for graphene-based terahertz antenna using the PEEC method," *IEEE Transactions on Antennas and Propagation*, vol. 64, no. 4, pp. 1385–1393, 2016.

[44] I. Llatser, C. Kremers, D. N. Chigrin, J. M. Jornet, M. C. Lemme, A. Cabellos-Aparicio, and E. Alarcon, "Radiation characteristics of tunable graphennas in the terahertz band," *Radioengineering*, vol. 21, no. 4, pp. 946–953, 2012.

[45] J. Christensen, A. Manjavacas, S. Thongrattanasiri, F. H. Koppens, and F. J. García de Abajo, "Graphene plasmon waveguiding and hybridization in individual and paired nanoribbons," *ACS nano*, vol. 6, no. 1, pp. 431–440, 2011.

[46] D. Correas-Serrano, J. S. Gomez-Diaz, J. Perruisseau-Carrier, and A. Alvarez-Melcon, "Graphene-based plasmonic tunable low-pass filters in the terahertz band," *IEEE Transactions on Nanotechnology*, vol. 13, no. 6, pp. 1145–1153, 2014.

[47] A. Taflove and S. C. Hagness, *Computational Electrodynamics*. Artech House, 2005.

[48] P.-Y. Chen and A. Alu, "A terahertz photomixer based on plasmonic nanoantennas coupled to a graphene emitter," *Nanotechnology*, vol. 24, no. 45, p. 455202, 2013.

[49] L. Falkovsky and A. Varlamov, "Space-time dispersion of graphene conductivity," *The European Physical Journal B-Condensed Matter and Complex Systems*, vol. 56, no. 4, pp. 281–284, 2007.

[50] S. Gevorgian and H. Berg, "Line capacitance and impedance of coplanar-strip waveguides on substrates with multiple dielectric layers," 2001.

[51] K. J. Binns and P. J. Lawrenson, *Analysis and Computation of Electric and Magnetic Field Problems: Pergamon International Library of Science, Technology, Engineering and Social Studies*. Elsevier, 2013.

[52] I. S. Gradshteyn and I. M. Ryzhik, *Tables of Integrals, Series, and Products*, 6th ed. Academic Press, 2000.

[53] M. Tamagnone, J. S. G. Diaz, J. Mosig, and J. Perruisseau-Carrier, "Hybrid graphene-metal reconfigurable terahertz antenna," in *2013 IEEE MTT-S International Microwave Symposium Digest (MTT)*, pp. 1–3, 2013.

[54] S. Abadal, S. E. Hosseininejad, A. Cabellos-Aparicio, and E. Alarcón, "Graphene-based terahertz antennas for area-constrained applications," in *2017 40th International Conference on Telecommunications and Signal Processing (TSP)*, pp. 817–820, 2017.

[55] D. Turan, S. C. Corzo-Garcia, E. Castro-Camus, and M. Jarrahi, "Impact of metallization on the performance of plasmonic photoconductive terahertz emitters," in *2017 IEEE MTT-S International Microwave Symposium (IMS)*, pp. 575–577, 2017.

[56] F. E. Terman, *Radio Engineers' Handbook*. McGraw-Hill Book, 1943.

[57] M. J. D. Powell, *Approximation Theory and Methods*. Cambridge University Press, 1981.